Analysis of PS-to-PP amplitude ratios for seismic reflector characterisation: method and application

N. Maercklin, A. Zollo
RISSC, Italy

Abstract: Elastic parameters derived from seismic reflection data provide information on the lithological contrast at an interface and support the geological interpretation. We present a method to estimate elastic parameter contrasts at a given interface in a 1-D layered medium from PS-to-PP amplitude ratios. The method is applied to synthetic data to demonstrate its possibilities and limitations. First results for real data acquired in the Campi Flegrei caldera (southern Italy) reveal a gas-bearing layer at around 3 km depth and indicate a strong negative velocity contrast at 7.5 km depth, possibly related to the presence of partial melt.

Introduction

Elastic parameters derived from seismic data can be related to the rock type, porosity, and fluid or gas content through empirical relationships and rock physics modelling (e.g. Avseth et al., 2005). Seismic first-arrival travel time tomography leads to a smooth image of the subsurface velocity structure, and ray modelling, reflection tomography, or depth migration can provide depths of reflectors and their topography. Seismic reflection amplitudes carry information on the elastic parameter contrasts at the reflectors itself. Amplitude variation with offset (AVO) or incident angle (AVA) analyses are standard tools in exploration seismics to estimate these contrasts. Typically, these methods are applied to PP reflection amplitudes and employ approximations to the Zoeppritz (1919) equations controlling the reflection amplitude variation with incidence angle. The relationships between physical rock properties and P-wave seismic data are highly non-unique, but an additional analysis of S-wave data may increase the ability to extract lithology and fluid effects from seismic data, because S-waves do not propagate through fluids (e.g. Veire and Landrø, 2006).

Standard AVO or AVA methods are applied to reflection coefficients, and therefore source, receiver, and propagation effects must be removed from the sei-

smic data before the analysis. Furthermore, the approximations made for the Zoeppritz equations are often valid for small incidence angles (small source-receiver offsets) and weak elastic contrasts only. For a given source-receiver offset, amplitude ratios between PS and PP reflected waves depend mostly just the elastic parameters at the reflector of interest, and total ray theoretic amplitudes can overcome the limitations of the approximate equations. This report presents a technique to analyse PS-to-PP amplitude ratios for arbitrary elastic contrasts using a wide range of source-receiver offsets. The method is introduced along with synthetic examples and applied to two major reflectors observed in the Campi Flegrei caldera, southern Italy.

Analysis method

A 1-D layered subsurface model is assumed, in which a constant P-velocity Vp, a P-to-S velocity ratio Vp/Vs, and a density ρ is assigned to each layer (Figure 1a). Six elastic parameters (Vp, Vp/Vs, ρ above and below a reflector) or three parameter contrasts characterise a given reflector. Ignoring anelastic attenuation and anisotropy, the amplitudes of primary PP and PS reflected phases (Figure 1b) depend on the source amplitudes and receiver site effects, on the geometrical spreading, and on the reflection coefficients at the reflector of interest. The reflection coefficients are a function of the elastic parameter contrasts and the incidence angles at the reflecting interface (Zoeppritz, 1919). We model the PP and PS amplitudes using ray theory, thereby including not only the effect of the elastic parameter contrast at the reflector but also the propagation effects in the overburden.

PS-to-PP amplitude ratios

The solid ray paths shown in Figure 1b for PP and PS connect the same source and receiver. Considering the ratio between the PS and PP amplitude for this acquisition geometry, the effects of source and receiver on the observed amplitudes are cancelled. Also the effect of geometrical spreading is reduced, and the exact dependency is accounted for in the ray theoretical forward modelling. Thus, measured PS-to-PP amplitude ratios provide a means to estimate the elastic parameters at the reflector without the need for additional amplitude correction factors.

Whereas PP is reflected at the midpoint (CMP) between source and receiver, the corresponding PS reflection lies closer to the receiver (Figure 1b). The asymmetry of the PS ray path depends on the Vp/Vs ratios in the layers above the reflector, and the distance between CMP and PS reflection point increases with increasing source-receiver offset and decreasing reflector depth. If the elastic parameter contrast at the reflector is varying laterally, the ratio

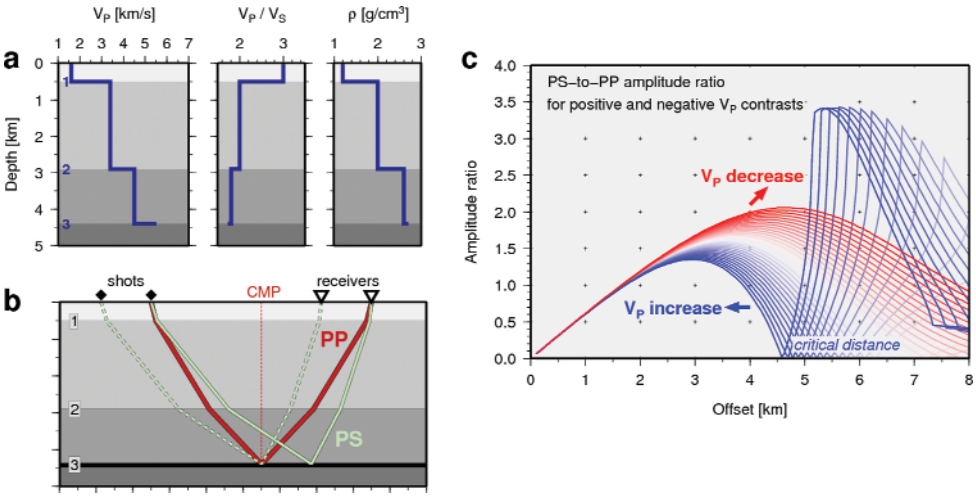

Fig. 1. **(a)** A layered 1-D velocity and density model. **(b)** Ray paths for primary PP and PS reflections from interface 3, recorded at the same source-receiver offset. **(c)** PS-to-PP amplitude ratios as a function of source receiver offset for positive P-velocity contrasts (blue) and negative contrasts (red) at interface 3. Successive lines correspond to a 2% velocity increase or decrease relative to the P-velocity in the layer above the interface.

between PS and PP reflected at the same subsurface location must be considered instead of the ratio calculated for the same source and receiver. An additional, laterally shifted source and receiver pair can provide the required PS observation (dashed PS ray path in Figure 1b). However, in this case the source amplitudes and possible receiver site effects have to be normalised before the calculation of the PS-to-PP ratio.

Figure 1c shows example PS-to-PP amplitude ratio curves as a function of offset for interface 3 of the model shown in Figure 1a. The ratios are calculated for a common offset of PS and PP. The blue lines are for models with a positive P-velocity contrast at that interface (*Vp* increase in the layer below the reflector), and the red curves are related to models with a negative contrast (*Vp* decrease). The maximum P-velocity contrast is 30% relative to *Vp* in the layer above the reflector. The general shape of the amplitude ratio variation with offset is dominated by the amplitude behaviour of the PS reflection. Due to a vanishing PS amplitude at zero offset, also the PS-to-PP ratio is always zero for coinciding source and receiver locations. The curves for the positive *Vp* contrast approach zero again at the distance of critical reflection, followed by a rapid increase of the amplitude ratio at post-critical distances. In case of a negative velocity contrast a critical reflection does not exist, resulting in smooth amplitude ratio curves with one single peak.

The six elastic parameters above and below a reflector are not independent. Generally, a higher value for a parameter in the layer above the reflector requi-

res also a corresponding higher one in the layer below to fit a given PS-to-PP amplitude ratio curve. This means that PS-to-PP ratio analysis essentially provides elastic parameter contrasts at a reflector, and some parameters must be constrained or fixed during an inversion. Furthermore, there is a trade-off between P-velocity and density, where the product of velocity and density, i.e. the seismic impedance, is constant. However, for a positive impedance contrast this trade-off can be resolved, if the critical distance depending only on the Vp contrast is observed.

Generic processing sequence

The observational basis for the analysis are travel times and amplitudes of PP and PS reflected at the same interface. The amplitudes must be extracted from seismograms at several source-receiver offsets covering a distance range large enough for a significant PS-to-PP amplitude ratio variation with offset, e.g. about 5 km for the example shown in Figure 1. We constrain the velocity structure above the reflecting interface by travel time modelling and assign initial values for the densities. Then we calculate PS-to-PP amplitude ratios at common offsets of PP and PS using seismic ray theory. Finally, we vary the unconstrained model parameters to minimise the RMS misfit between observed and theoretical amplitude ratio curves. The minimisation process is a grid search through the model parameter space, possibly combined with simplex optimisation to find a local minimum of the misfit function. Slices through the parameter space showing the misfit value as a function of selected model parameters provide an estimate of the uncertainty of the solution.

Synthetic case study

A dipping reflector and a laterally varying overburden violates the assumption of a 1-D model. To illustrate these effects on the analysis of PS-to-PP amplitude ratios, we apply our method to amplitude ratios extracted from synthetic data for a hypothetical volcanic caldera structure (Figure 2a). The target of this case study is a segment of the deepest reflector in the 2-D model. The subsurface structure above the target shows lateral variation, and the target reflector itself is dipping toward the left side of the profile (Figure 2a). The data to be analysed are vertical and horizontal component seismograms calculated for a line of shots in a shallow water layer and recorded at a single receiver at the sea bottom (common receiver gather). Primary PP and PS reflections from all model interfaces are included in the synthetics. The use of this acquisition geometry is justified, because the shot amplitudes are all the same and the elastic parameter contrasts at the reflector are nearly homogeneous.

First, we construct an approximate 1-D velocity model from the PP and PS travel times of the target reflector and of the three reflectors above (see Figure 2b, top). The densities for each layer are taken from the 2-D model. Second, we measure the PP amplitudes for the target reflector from the vertical component seismograms and the corresponding PS amplitudes from the horizontal sections, excluding those parts of the reflection signal that is contaminated by other phases. Third, theoretical PS-to-PP amplitude ratios for this model are fit to the measured curve by varying *Vp*, *Vp*/*Vs*, and the den-

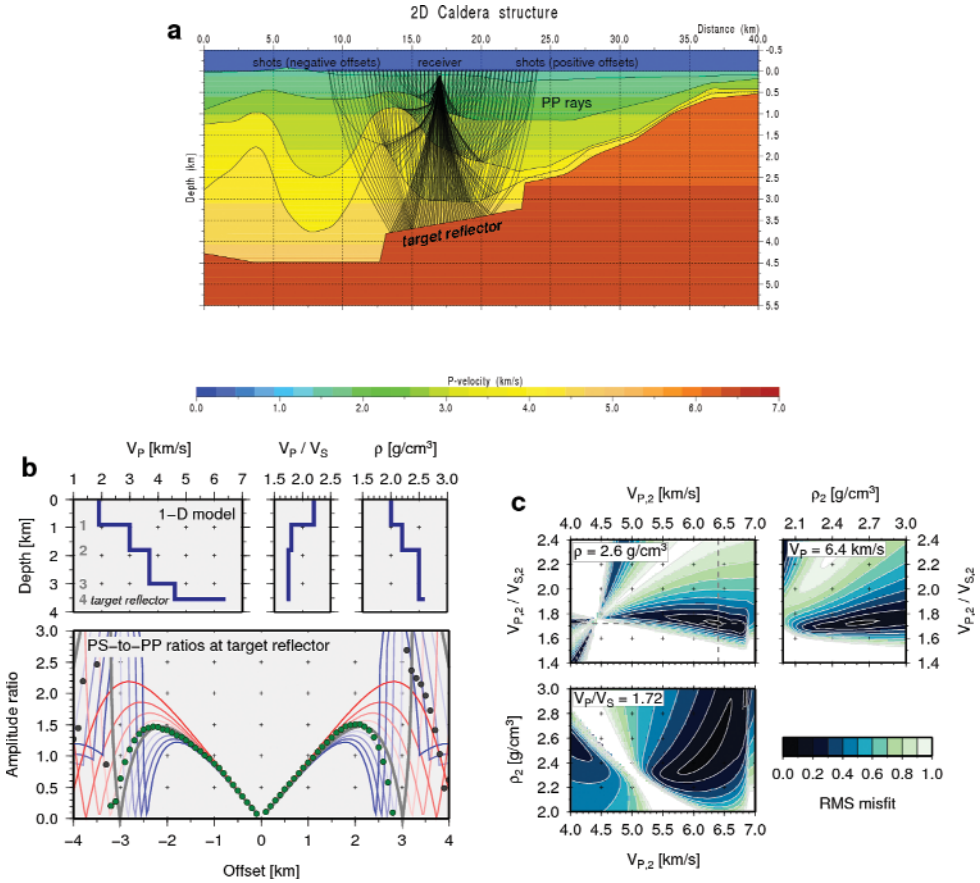

Fig. 2. (a) P-velocity profile through a hypothetical caldera structure and PP ray paths for a common receiver gather. **(b)** Approximate 1-D model based on travel times for the common receiver gather. The *Vp/Vs* ratios and densities are the same as in the 2-D model. The bottom panel shows synthetic PS-to-PP amplitude ratio curves (lines) overlain with pre- (green dots) and post-critical (grey dots) amplitude ratios. The grey line is the theoretical curve for the model shown above, and blue and red lines correspond to models with higher and lower P-velocity in the layer below the target reflector (maximum variation of 20%). **(c)** Slices through the parameter space for the model parameters in the layer below the target reflector.

sity in the layer below the reflector. Here, the PS-to-PP ratio curve is an average of that for negative offsets (shots on the left of the receiver) and that for positive offsets (shots on the right).
Figures 2b and 2c summarise the results of the PS-to-PP amplitude ratio analysis outlined above. Figure 2b is an overlay plot of the measured amplitude ratios (dots) and a theoretical curve for the best fitting model obtained with the density contrast fixed to the known value (grey line). The additional blue and red curves are for alternative models with higher and lower Vp contrasts, respectively. The critical distance for the estimated (and true) P-velocity contrast ΔVp=1.8 km/s (39% increase) is reached at an offset of about 3 km. Measured pre-critical amplitude ratios (green dots in Figure 2b) are fit well by the theoretical values. For the positive offset branch the measured amplitude ratios approach zero at a smaller offset than the theoretical curve, which suggests a higher Vp contrast than that of the optimum 1-D average model. The opposite observation is made for the negative offset branch. Post-critical amplitude ratios are much more sensitive to small changes of elastic parameters and incidence angles. Measured post-critical amplitude ratios and the theoretical values for the approximate 1-D model do not match because of the reflector dip and the lateral velocity variation in the overburden. Here, a reasonable fit is only obtained for the large post-critical PS-to-PP amplitude ratios at offsets up to about 3.4 km, i.e. at offsets exceeding the critical distance only slightly.
Figure 2c illustrates the resolution of the estimated elastic parameters below the target reflector. Each of the three panels shows the RMS misfit between the measured pre-critical PS-to-PP amplitude ratios and the theoretical values as a function of two elastic parameters for the layer below the reflector. The third parameter for the layer below and the three parameters of the layer above are kept constant at the value of the best model (Figure 2b, top). The dark regions in these slices through the model parameter space outline elastic parameter combinations that yield a good fit, i.e. a narrow dark region indicates a better resolution of the related parameter than a wide region of possible values. In the panel for Vp and ρ (bottom left) the trade-off between these two parameters is clearly visible as a large region of probable Vp-ρ pairs. A similar but less pronounced parameter correlation can be seen in the other two panels (Vp/Vs versus Vp and ρ versus Vp/Vs). An uncertainty of 10-15% for each estimated elastic parameter may be assigned here.

Application to the Campi Flegrei caldera

During the SERAPIS controlled-source seismic experiment in 2001 (e.g. Zollo et al., 2003) a large number of airgun shots was recorded by a grid of three-component ocean bottom seismometers (OBS) deployed in the Bay of Pozzuoli (Figure 3a), which covers a part of the Campi Flegrei caldera. The average water depth at the OBS locations is about 100 m, and the orientation

of their horizontal components have been determined by polarisation analysis of the direct wave travelling in the water layer.
We identified three major reflectors on several common midpoint (CMP) gathers from this dataset, and the travel times of PP and PS arrivals from each reflector were picked. The association of the PP phase and the PS phase from the same interface is based on travel time modelling for a layered 1-D average velocity model (Vp and Vp/Vs) and on reflection move-out analysis. The PP and PS travel time picks used here are shown in Figure 3b together with theoretical travel times of PP (solid lines) and PS (dashed lines) for the preliminary 1-D model derived from travel time modelling and the amplitude ratio analyses described below (see Figure 5). The maximum offsets considered here are 2 km for the shallowest reflector and up to 8 km for the deeper ones.
As in the synthetic case study, we extracted the PP amplitudes from vertical component seismograms and corresponding PS amplitudes from radial sections constructed from the two horizontal OBS components. We applied a 5-15 Hz bandpass filter and measured the amplitudes in a time window of 0.2 s around the maximum of the respective arrival. Since the measured amplitudes exhibit a large variation, we smoothed the amplitude variation with offset for each phase by taking the median value in 0.25 km wide offset bins. Then we calculated the PS-to-PP amplitude ratios at common offsets for PP and PS for two interfaces (Figure 3c).

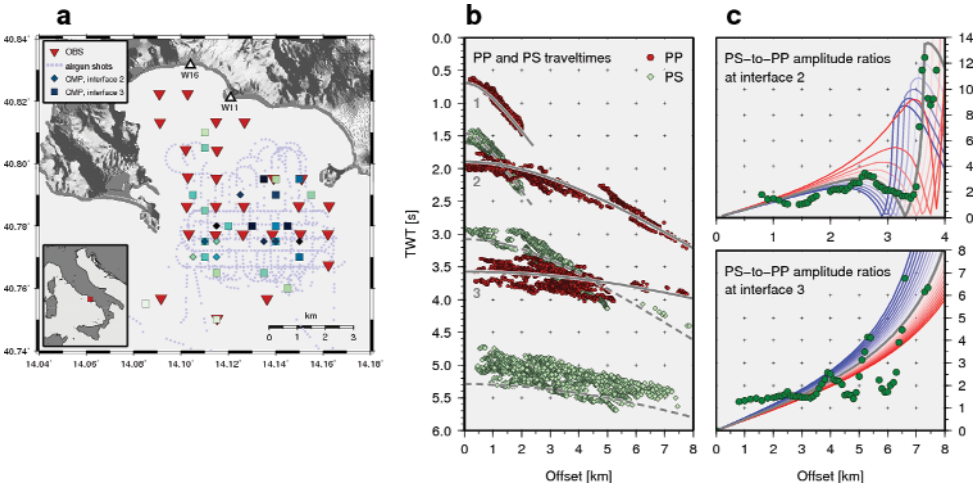

Fig. 3. **(a)** Map of the seismic acquisition geometry used. A higher number of available PP amplitude measurements is indicated by darker colours of the CMP symbols. **(b)** PP and PS travel time picks (dots) for three major reflectors overlain with theoretical times (grey lines) from a 1-D average model. **(c)** Average of the observed amplitude ratio variation with offset (dots) for two reflectors (interfaces). Theoretical curves for the 1-D model (Figure 5) are shown as grey lines. The blue and red curves are for models with higher and lower *Vp* in the layer below the respective interface (2% interval).

The PS-to-PP amplitude ratios (dots) plotted in Figure 3c are the average of all measured PS-to-PP amplitude ratios available for the respective interface. A decrease of PS-to-PP ratios is observed for interface 2 at around 3.3 km offset, followed by a rapid increase toward greater offsets. This behaviour suggests a well-constrained positive *Vp* contrast at that interface. The PS-to-PP ratio variation with offset for interface 3 is undulating, but it shows a tendency for an increase of PS-to-PP ratios with offset.

Grey lines in Figure 3c are the theoretical PS-to-PP amplitude ratio curves that fit the general trend of the observed ratios. The used 1-D velocity model is based on travel time modelling and on *Vp* and *Vp/Vs* below the respective interface estimated from the amplitude ratios. Density contrasts are not included in the modelling (ρ=2.6 g/cm^3 within each layer). Slices through the model parameter space illustrate the resolution of the obtained 1-D model. Figure 4 shows the colour-coded RMS misfit between observed and theoretical amplitude ratios as a function of two elastic parameters in the layer below the reflector while keeping the remaining parameter constant at the value printed in each panel.

The misfit function for interface 2 at 2.7 km depth shows a narrow minimum in the plane of *Vp/Vs* versus *Vp* (Figure 4a, top left). Thus, the measured PS-to-PP amplitude ratios provide a good estimate of the P-velocity contrast at this interface. A variation of ρ does not have a significant influence on *Vp* (bottom left), and also *Vp/Vs* depends only slightly on the value of (top right). A different pattern is found for interface 3 at 7.5 km depth (Figure 4b). Several combinations of *Vp* and *Vp/Vs* for the layer below yield the same RMS misfit between measured and theoretical curves (top left panel), and also several density values are possible. Since the layer above interface 3 has a P-

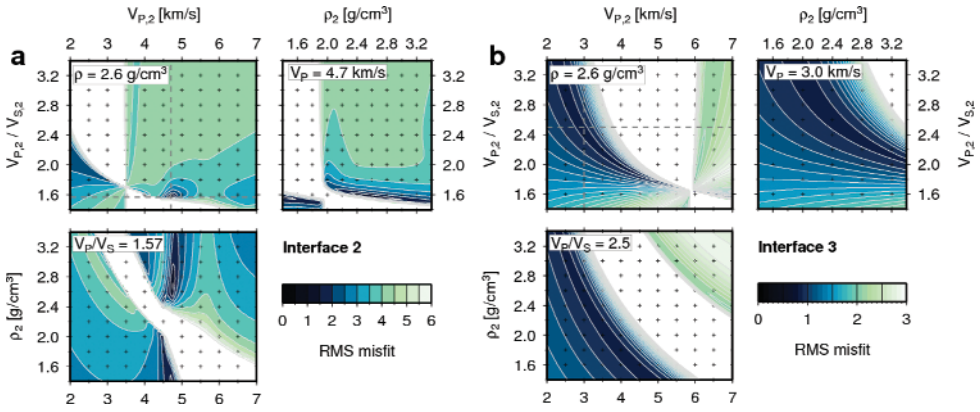

Fig. 4. Slices through the model parameter space for two interfaces showing the colour-coded RMS misfit as a function of two model parameters for the layer below the interface while keeping the remaining parameter constant at the value given in each panel. See Figure 5 for the velocities above the interfaces.

velocity of Vp=5.9 km/s, a good fit is typically requires a negative velocity contrast at this interface.

Figure 5 summarises the preliminary 1-D velocity model obtained from the combined travel time and PS-to-PP amplitude ratio analyses assuming a constant density. The shallowest layer is characterised by a low P-velocity and a high Vp/Vs ratio (Vp=1.6 km/s, Vp/Vs=3.4). Large amplitudes of PP and PS reflections from interface 1 suggest a strong Vp and Vp/Vs contrast at this interface (0.6 km depth), but their actual values may be smaller than shown here due to a probably velocity gradient in the first layer. At interface 2 the P-velocity increases from 3.5 km/s to 4.7 km/s, accompanied with a Vp/Vs decrease from 1.7 to 1.57. Another model discontinuity introduced at 3.3 km depth is not observed in the reflection data, but a further, most likely gradual Vp increase to about 5.9 km/s is required to fit the travel times from the deepest reflector (interface 3). The results of the PS-to-PP amplitude ratio modelling indicate a strong negative Vp contrast and an even higher Vs contrast (Vp/Vs increase) at interface 3 in 7.5 km depth. The 1-D P-velocity and Vp/Vs model presented here is consistent with the 1-D average from a 3-D P-velocity model for the study region (Zollo et al., 2003), and Vanorio et al. (2005) derived similar Vp/Vs ratios at stations located near our study region.

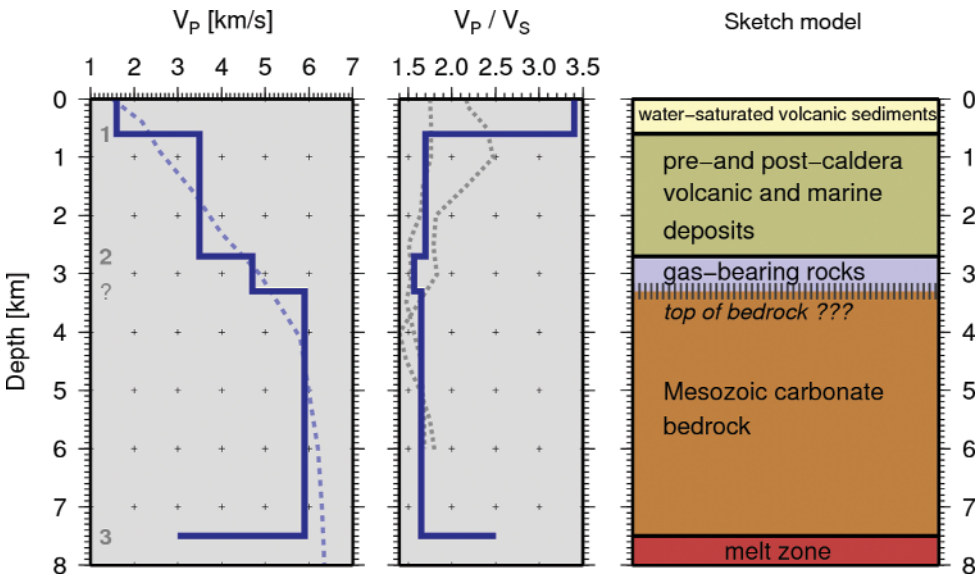

Fig. 5. Average 1-D P-velocity and *Vp/Vs* model for the Campi Flegrei caldera, based on PP and PS travel times, and on PS-to-PP amplitude ratios. The dashed line is the average of a 3-D P-velocity model in the study area (Zollo et al., 2003), and the dotted lines are *Vp/Vs* profiles derived by Vanorio et al. (2005) at the stations W16 and W11 (Figure 3a).

Discussion and conclusions

The PS-to-PP amplitude ratio analysis described above yields elastic parameter contrasts at reflectors using wide-angle reflection data, and the method does not require additional amplitude correction factors as needed for standard AVO techniques. However, at small offsets the PS-to-PP amplitude ratios do not change significantly with the *Vp* contrast at the reflector (Figures 1c and 2b). Additionally, noise in real data has a stronger influence on the small PS amplitudes at short offsets and may introduce a systematic bias toward higher PS-to-PP ratios. Therefore, amplitude ratio measurements are needed for sufficiently large offsets. In this case, the method is applicable also to subsurface structures that violate the 1-D assumption by a slightly dipping reflector or a laterally varying overburden (Figure 2). If the critical distance is observed, the positive *Vp* contrast is well-resolved, and also a good estimate for *Vp*/*Vs* can be expected. Generally, the recovery of density contrasts may require additional constraints e.g. from empirical velocity-density relations.

As for all AVO/AVA methods using PP and PS simultaneously, these two phases must be identified for the same reflector. The most reliable association between the two phases can be made from well log data. Due to the lack of such information for the deeper layers in the Campi Flegrei caldera, we guided the search for corresponding PP and PS phases by travel time modelling. In an alternative approach that does not require PP and PS from the same interface, Auger et al. (2003) used amplitude ratios between PS reflections and the first-arrival P-wave.

We successfully applied the PS-to-PP amplitude ratio analysis to two reflectors in the Campi Flegrei caldera. Main features of the observed amplitude ratio curves are reproduced by our preliminary 1-D model assuming a vanishing density contrast (Figure 5). The 1-D velocity structure is consistent with the PP and PS travel times for three interfaces and with a 3-D P-velocity model from first-arrival tomography (Zollo et al., 2003). The sketch model in Figure 5 summarises our tentative interpretation of the model. A layer of water-saturated volcanic sediments from the recent activity covers a succession of pre-and post-caldera deposits. Vanorio et al. (2005) interpreted regions with low *Vp*/*Vs* ratios in the study region as gas-bearing rocks, and the observed amplitude ratios provide evidence for such a layer at around 3 km depth. The thickness of this layer and the transition to the Mesozoic carbonate basement remains unresolved. Following an interpretation by Auger et al. (2003) for a similar observation beneath Vesuvius volcano, a strong negative velocity contrast at 7.5 km depth may be related to partially molten rock in the layer below.

REFERENCES

Auger, E., Virieux, J., and Zollo, A. (2003). Locating and quantifying the seismic discontinuities in a complex medium through the migration and AVA analysis of reflected and converted waves: an application to the Mt. Vesuvius volcano. Geophysical Journal International, 152(2), 486-496.

Avseth, P., Mukerji, T., and Mavko, G. (2005). Quantitative seismic interpretation: Applying rock physics tools to reduce interpretation risk. Cambridge University Press, Cambridge, UK.

Vanorio, T., Virieux, J., Capuano, P., and Russo, G. (2005). Three-dimensional seismic tomography from P wave and S wave microearthquake travel times and rock physics characterization of the Campi Flegrei Caldera. Journal of Geophysical Research, 110, B03201, doi:10.1029/2004JB003102.

Veire, H. H. and Landrø, M. (2006). Simultaneous inversion of PP and PS seismic data. Geophysics, 71(3), R1-R10.

Zoeppritz, K. (1919). Erdbebenwellen VII b: über Reflexion und Durchgang seismischer Wellen durch Unstetigkeitsflächen. Nachrichten von der Gesellschaft der Wissenschaften zu Göttingen, Mathematisch-Physikalische Klasse, 1919, 66-84.

Zollo, A., Judenerc, S., Auger, E., D'Auria, L., Virieux, J., Capuano, P., Chiarabba, C., de Franco, R., Makris, J., Michelini, A., and Musaccio, G. (2003). Evidence for the buried rim of Campi Flegrei caldera from 3-d active seismic imaging. Geophysical Research Letters, 30(19), 2002, doi:10.1029/2003GL018173.